JACS
JOURNAL OF THE AMERICAN CHEMICAL SOCIETY
Article
pubs.acs.org/JACS

Electrocatalytic Oxygen Evolution at Surface-Oxidized Multiwall Carbon Nanotubes

Xunyu Lu,[†] Wai-Leung Yim,[‡] Bryan H. R. Suryanto,[†] and Chuan Zhao*[,†]

[†]School of Chemistry, The University of New South Wales, Sydney, New South Wales 2052, Australia

[‡]Institute of High Performance Computing, Agency for Science, Technology, and Research, 1 Fusionopolis Way, No. 16-16 Connexis, Singapore 138632

Supporting Information

ABSTRACT: Large-scale storage of renewable energy in the form of hydrogen (H_2) fuel via electrolytic water splitting requires the development of water oxidation catalysts that are efficient and abundant. Carbon-based nanomaterials such as carbon nanotubes have attracted significant applications for use as substrates for anchoring metal-based nanoparticles. We show that, upon mild surface oxidation, hydrothermal annealing and electrochemical activation, multiwall carbon nanotubes (MWCNTs) themselves are effective water oxidation catalysts, which can initiate the oxygen evolution reaction (OER) at overpotentials of 0.3 V in alkaline media. Oxygen-containing functional groups such as ketonic C═O generated on the outer wall of MWCNTs are found to play crucial roles in catalyzing OER by altering the electronic structures of the adjacent carbon atoms and facilitates the adsorption of OER intermediates. The well-preserved microscopic structures and highly conductive inner walls of MWCNTs enable efficient transport of the electrons generated during OER.

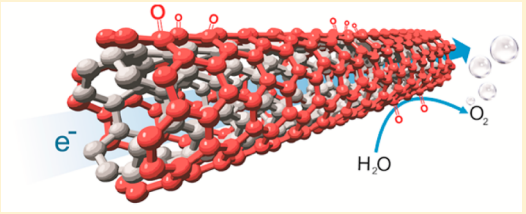

INTRODUCTION

Electrolytic water splitting holds the promise for global scale storage of renewable energy, e.g., solar and wind in the form of hydrogen fuel, enabling the continuous usage of these intermittent energy sources when used together with fuel cells.[1,2] However, the sluggish kinetics of oxygen evolution reaction (OER) on the anode often requires catalyst materials such as oxides of iridium (IrO_2) and ruthenium (RuO_2) to lower the energy barriers of OER so that hydrogen can be generated at the cathode with appreciable rate at relatively low applied voltages. However, the noble metal based catalysts are costly and their supply is not sustainable, which has severely restricted the large-scale implementation of this technology.[3−5] Recently, significant research efforts have gone to the development of efficient OER catalysts based on oxides of first-row transition metals, such as Ni, Fe, Co and Mn.[6−9] Transition metal oxides generally have intrinsically low conductivity, and the issue aggravates when nanoparticles of the metal-oxides are used to enhance the catalytic sites. To circumvent this issue, nanoparticles of transition metal oxides are normally anchored onto conductive substrates such as carbon nanomaterials, e.g., graphene and multiwall carbon nanotubes (MWCNTs).[8−11] Such a design introduces large amounts of available catalytic sites and efficient charge transport, and the obtained composite catalysts exhibit enhanced catalytic activity toward OER, with some comparable to the benchmark Ir/C catalyst.[12]

More recent developments include the so-called "metal-free" catalysts based on deliberate doping of heteroatoms, e.g., nitrogen and boron, into the graphitic network that can alter the chemical and electronic properties of nanocarbons for desired applications.[13−15] In particular, being low cost metal-free catalysts for oxygen reduction reaction (ORR) and OER, nitrogen doped carbon nanomaterials have gained significant popularity recently. In the applications of nanocarbon materials, both as supports for metal nanoparticles or as metal-free OER catalysts themselves, the coexistence of oxygen-containing groups on the carbon materials is almost inevitable. This is because the oxidation of the nanocarbon substrates is usually required to introduce oxygen-containing groups and defect sites for subsequent functionalization or doping with heteroatoms. However, the role of oxygen-containing groups on the catalytic activity remains unclear.

Herein, we show that unexpectedly high OER catalytic activity can be achieved by using surface-oxidized and electrochemically activated MWCNTs. Unlike previously reported carbon-based catalysts, the oxidized MWCNTs consisted of only C and O on the surface, which enables us to study the role of O in catalyzing OER. This study reveals for the first time that the significant role of oxygen-containing groups, especially ketonic (C═O) groups, as the catalytic active sites for OER. Hence, by rational design, carbon nanomaterials bearing oxygen-containing groups can be utilized as a new category of efficient OER catalysts.

EXPERIMENTAL SECTION

Preparation of Surface-Oxidized MWCNTs (o-MWCNTs). *Preparation of Mildly Oxidized MWCNTs.* Piranha solution treated MWCNTs were prepared by adding MWCNTs (100 mg) into piranha

Received: September 25, 2014
Published: February 6, 2015

DOI: 10.1021/ja509879r
J. Am. Chem. Soc. 2015, 137, 2901−2907

solution (10 mL, 7 mL of 98% H_2SO_4 and 3 mL of 30% H_2O_2) in a round-bottom flask (50 mL). The mixture was stirred gently at 22 °C for 5 h (for MWCNTs made from Fe catalysts, the mixture was stirred at 45 °C overnight), and diluted with copious amount of water. MWCNTs were collected by filtration and washed thoroughly with water and ethanol, and then dried under vacuum overnight.

Preparation of Weakly Oxidized MWCNTs. 100 mg of MWCNTs were added into 12 mL of 36% HCl solutions in a 50 mL round-bottom flask. The mixture was stirred for 2 h, and collected by filtration and washed thoroughly with water and ethanol, and then dried under vacuum overnight.

Preparation of Strongly Oxidized MWCNTs. 100 mg of MWCNTs were mixed with 3 mL of 65% HNO_3 and 9 mL of 98% H_2SO_4 in a 50 mL round-bottom flask, and stirred at 75 °C for 3 h. The reaction mixture was then diluted with copious amount of water, filtrated and washed thoroughly with water and ethanol. The resulting MWCNTs were collected after drying under vacuum overnight.

Hydrothermal Treatments of Oxidized MWCNTs (ho-MWCNTs). The as-obtained o-MWCNTs were resuspended in water by a brief sonication, and added into a 48 mL Teflon-lined autoclave, which was subsequently underwent a hydrothermal reaction at 180 °C overnight. MWCNTs were collected by repeated centrifugation and washing with water.

Electrochemical Activation (echo-MWCNTs). One mg of ho-MWCNTs were dispersed in 0.2 mL of ethanol/water (1:1, v/v) followed by the addition of 10 μL of Nafion (5 wt %, Sigma-Aldrich). The mixture was sonicated for 15 min to form a homogeneous ink. Subsequently, 3 and 5 μL of the ho-MWCNTs ink was loaded onto the surface of glassy carbon macrodisc electrode and glassy carbon rotating disk electrode (RDE), respectively. Then, echo-MWCNTs were obtained by cycling the ho-MWCNTs loaded electrodes continuously in a 0.1 M KOH solution in the potential range of 0−0.8 V vs Ag/AgCl, until stabilized current for OER was established.

Preparation of Fe-Modified MWCNTs. The Fe nanoparticle modified MWCNTs were prepared according to the established method.[8,11] Briefly, MWCNTs prepared from Fe catalysts (Mitsui, Japan) were first stirred gently in the piranha solution for 5 h, which were collected and redispersed in absolute ethanol to form a suspension of 0.66 mg mL^{-1}. Then, 0.54 mL of 0.2 M iron acetate and 0.54 mL of 28% $NH_3.H_2O$ were subsequently added into the MWCNT suspension, and refluxed at 80 °C for 12 h before transferring into an autoclave for hydrothermal reactions at 150 °C for 3 h. The Fe-modified MWCNTs products were collected by repeated centrifugation and washing with water.

Preparation of Thermally Reduced ho-MWCNTs. Thermally reduced ho-MWCNTs were prepared under an argon environment, and subsequently heated to 1000 °C at the ramping rate of 5 °C min^{-1}. After reaching 1000 °C, the cell was allowed to cool naturally and the samples were collected without further treatments.

Physical Characterization. SEM images were obtained from FEI Nova NanoSEM 230 at 3 kV. Samples were prepared by drop casting their ethanol suspensions onto conductive substrates. TEM images were obtained from Philips CM 200 at 200 kV with samples prepared by drop casting their diluted ethanol solutions onto copper grids. XPS characterizations were carried out on Thermo ESCALAB250i X-ray Photoelectron Spectrometer. Samples were prepared by drop-casting MWCNTs directly onto the carbon fiber paper substrate without using Nafion binders. The inductively coupled plasma mass spectrometry (ICP-MS) characterization of MWCNTs samples were performed on a PerkinElmer Quadrupole Nexion ICPMS. Samples for ICP-MS test were prepared by dissolving a known amount of MWCNTs in 2 mL of nitric acid (TraceSELECT, Sigma-Aldrich). The reaction mixture was then digested using a CEM Discovery SP with Explorer SP Autosampler microwave reactor (CEM) at 30 W for 4 h. During digestion, the upper temperature limit was set at 180 °C.

Electrochemical Procedures. One mg of the treated MWCNTs were dispersed in water and ethanol solution (0.2 mL, 1:1, v/v), followed by the addition of Nafion. The mixture was sonicated for 15 min to form a stable and homogeneous MWCNT ink. 3 and 5 μL of the ink were drop casted onto the surface of glassy carbon electrode and RDE, respectively, and left to dry in air. For bulk water electrolysis, the MWCNTs loaded Teflon-line carbon fiber paper (CFP, Fuel Cell Store) and nickel foam (Goodfellow) were prepared using the similar method with much higher MWCNTs loading at 1 mg cm^{-2}. Voltammetric measurements were carried out using a CHI 760 Electrochemical Workstation (CH Instrument) with a standard three-electrode cell containing a MWCNT-decorated glassy carbon or RDE working electrode, a Ag/AgCl (3 M KCl) reference electrode, and a Pt mesh counter electrode. Potentials reported in this study were all quoted against the reversible hydrogen electrode (RHE) using equation $E_{RHE} = E_{Ag/AgCl} + 0.197 + 0.059 \times pH$, where E_{RHE} is the potential calibrated against RHE and $E_{Ag/AgCl}$ is the potential measured against the Ag/AgCl reference electrode. The polarization curves were recorded by linear sweep of potential at a scan rate typically of 5 mV s^{-1}. Unless specifically mentioned, all the polarization curves shown in the work are the second sweep, as the first sweeps are usually unstable and more affected by residual currents and large capacitance currents. All RDE voltammograms were recorded at a rotating rate of 1600 rpm. Unless specifically mentioned, RDE voltammograms were recorded with *iR* drop compensation, which was determined using the same potentiostat.

RESULTS AND DISCUSSION

The OER-active MWCNTs were prepared by sequential acid oxidation, hydrothermal annealing and in situ electrochemical activation of commercial MWCNTs. Initially, MWCNTs were stirred in piranha solutions (a mixture of 7/3 (v/v) 98% H_2SO_4 and 30% H_2O_2) at 22 °C for 5 h to afford mildly oxidized MWCNTs (o-MWCNTs). This step is known to introduce defect sites and oxygen containing groups onto pristine CNT surfaces and also remove the residual metal impurities to a great extent.[16] Compared with the raw MWCNTs, piranha solution-oxidized MWCNTs exhibited significantly increased oxygen content from 1.1 to 4.0 at. %, as revealed by X-ray photoelectron spectroscopy (XPS, Figure S1). The o-MWCNTs were subsequently transferred into a Teflon-lined autoclave for a hydrothermal treatment at 180 °C overnight. The oxygen content of o-MWCNTs has been reduced to 2.2 at. % after hydrothermal treatment (ho-MWCNTs) as a result of desorption of less-stable oxygen-containing groups. Finally, ho-MWCNTs were drop-casted onto a substrate electrode (e.g., glassy carbon), and activated by cycling the potential continuously in 0.1 M KOH between 0 and 0.8 V vs Ag/AgCl (3 M KCl) until stable current for OER was established. Electrochemical activation processes led to an increase of oxygen content of ho-MWCNTs up to 6.0 at. %. Transmission electron microscopy (TEM) investigation of the electrochemically activated ho-MWCNTs (echo-MWCNTs) showed no significant change of the morphology and structural integrity of the MWCNTs after the three-step treatments (Figure S2).

The OER activities of the o-MWCNTs, ho-MWCNTs and the electrochemically activated ho-MWCNTs (echo-MWCNTs) have been characterized in 0.1 M KOH by using a glassy carbon macrodisc working electrodes loaded with the corresponding MWCNT inks, a Pt counter electrode and a Ag/AgCl (3 M KCl) reference electrode. All the potentials quoted in the study are calibrated against a reversible hydrogen electrode (RHE) for the comparison purpose. Figure 1A represents the corresponding polarization curves obtained at each treatment stage. The OER catalytic activity increases with each step of the treatments, showing progressively lowered onset potentials for OER and significantly enhanced current densities, calculated using geometric surface area (j_{GSA}, GSA = geometric surface area), at a given potential (e.g., 1.75 V). The echo-MWCNTs exhibit the highest OER catalytic activity with an onset overpotential of merely 300 mV in 0.1 M KOH. Vigorous gas evolution is

DOI: 10.1021/ja509879r
J. Am. Chem. Soc. 2015, 137, 2901−2907

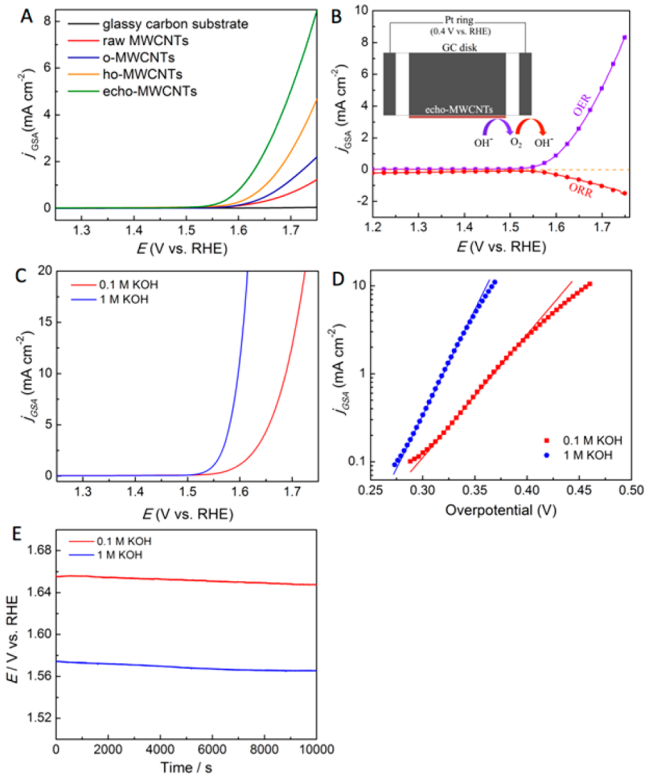

Figure 1. Electrochemical characterizations of the echo-MWCNTs for OER. (A) Polarization curves obtained with MWCNTs of different treatment stages coated glassy carbon electrodes in 0.1 M KOH at a scan rate of 5 mV s^{-1}. (B) Detection of O_2 evolution from the echo-MWCNTs catalysts using rotating ring disk electrode measurements (inset shows the schematic of RRDE detection). The oxygen generated during the anodic polarization scan is reduced at the Pt ring at a constant potential of 0.4 V. (C) RDE voltammogram obtained with the echo-MWCNTs in 0.1 and 1 M KOH solutions at a scan rate of 5 mV s^{-1} with *iR* compensation. (D) Tafel slopes derived from C. (E) Chronopotentiometric curves obtained in constant current (j = 5 mA cm^{-2}) bulk water electrolysis with echo-MWCNTs coated CFP in 0.1 and 1 M KOH solution.

observed on the surface of echo-MWCNTs-coated glassy carbon electrode after the onset potential (Figure S3A). The gas was verified to be oxygen, as the current for ORR in the subsequent cathodic scan is dramatically enhanced (Figure S3B). Furthermore, the gas evolution at echo-MWCNTs is characterized with a rotating ring disk electrode (RRDE) in argon-saturated 0.1 M KOH. The rotating Pt ring disk electrode is held at 0.4 V to quantify the oxygen evolved at the echo-MWCNTs modified glassy carbon disc electrode.[17] Figure 1B shows that prior to the potential of OER process, no current is detected at the Pt ring electrode for ORR. When the potential is scanned above the onset of OER (1.53 V), the ORR current at the ring electrode increases concomitantly with the oxidative current at the disc electrode, suggesting that the product at the disc electrode is oxygen. Changing the ring electrode potential to 1.4 V to monitor the production of H_2O_2 leads to no current detectable at the ring electrode (Figure S4), further confirming no H_2O_2 is generated and the water oxidation at echo-MWCNTs proceeds via a 4-electron transfer process to form dioxygen. The Faradaic efficiency, calculated by comparing the amount of oxygen detected at the ring electrode with the theoretical value using the charge consumed at the disk electrode, is close to unity (99%) (Figure S5), confirming oxygen is the only product of the electrode reaction.

The OER catalytic activity of the echo-MWCNTs were further characterized using glassy carbon rotating disk electrode (RDE) at 1600 rpm in 0.1 and 1 M KOH solutions, respectively. In 0.1 M KOH, the potential required to obtain j_{GSA} of 10 mA cm^{-2} is 1.68 V, corresponding to an overpotential (η) of 450 mV (Figure 1C). Even higher catalytic current is achieved in 1 M KOH solution (Figure 1C), as a result of reduced solution resistance,[12] delivering the j_{GSA} of 10 mA cm^{-2} at a lower η of 360 mV. This value is comparable with state-of-the-art transition OER catalysts based on metal oxides such as $Ni_{0.9}Fe_{0.1}O_x$ composite obtained in the same concentration of KOH electrolyte.[18] The high OER catalytic activity of the echo-MWCNTs was further confirmed by calculating the current density using electrochemically active surface area (j_{ECAS}, see calculation details in Supporting Information (SI) and Figure S6A,B), determined from the double layer capacitance.[19] At the η = 350 mV, the echo-MWCNTs delivers an OER j_{ECAS} of 0.14 mA cm^{-2} (Figure S6C), a value that is about 10 times higher than the electrodeposited CoO_x and CoPi composites,[20,21] and comparable to the time-honored NiO_x catalyst.[22] Figure 1D shows the Tafel plots of the echo-MWCNTs in OER derived from Figure 1C. In both 0.1 and 1 M KOH, the Tafel plots remained good linearity, indicating a good electrical conductivity retained with the echo-MWCNTs. The Tafel slopes obtained for the echo-MWCNTs are 72 and 41 mV dec^{-1} respectively, which are smaller than the previously reported values for nitrogen-doped nanoporous carbon catalysts,[15,23] and carbon and/or metal hybrids.[24−26]

To understand the unexpected electrocatalytic activity of echo-MWCNTs, it is essential to first elucidate the role of metal impurities in the MWCNTs. This is because that commercial MWCNTs are prepared from transition metal catalysts such as Ni or Fe, and the presence of metal impurities in MWCNTs is almost unavoidable. The metal impurities in MWCNTs can exist in two forms: residual metal on the MWCNT surface (exterior) and metal particles embedded inside MWCNTs (interior). In our case, the MWCNTs were prepared from Ni catalysts and thus nickel (Ni) was the major impurity of concern. Exterior Ni impurities on the MWCNT surface can be effectively removed by acid washing.[27] Extensive investigations of o-MWCNT samples using high resolution TEM (Figure S7A) and XPS reveal that treatment of MWCNTs by refluxing in piranha solution has effectively removed the exterior Ni impurities and the o-MWCNT surface is metal-free (<0.1 at. %) (Figure S1). In contrast, the complete removal of interior metal impurities is known to be almost impossible. Table S1 shows that ppm level of Ni can be detected in o-MWCNTs after refluxing in piranha solution by using inductively coupled plasma mass spectrometry (ICP-MS).[28,29] Shown also in TEM images (Figure S7B), Ni particles are found embedded inside the o-MWCNTs. Nevertheless, because the embedded Ni impurities are not in contact with electrolytes, they have little contribution to the OER activity, which is confirmed by the fairly low OER catalytic activity obtained with acid-washed o-MWCNTs (Figure 1A).

Electrochemical activation introduces significant amount of oxygen content onto the MWCNTs surface and lead to dramatically enhanced OER activity (Figure S8). One reasonable concern is that if the MWCNTs are etched during electrochemical oxidative activation, thus exposing the embedded Ni to electrolytes and contributing to the OER. Figure 2A and 2B represent the TEM images obtained after the electrochemical activation processes, which shows that the tube structures of

DOI: 10.1021/ja509879r
J. Am. Chem. Soc. 2015, 137, 2901−2907

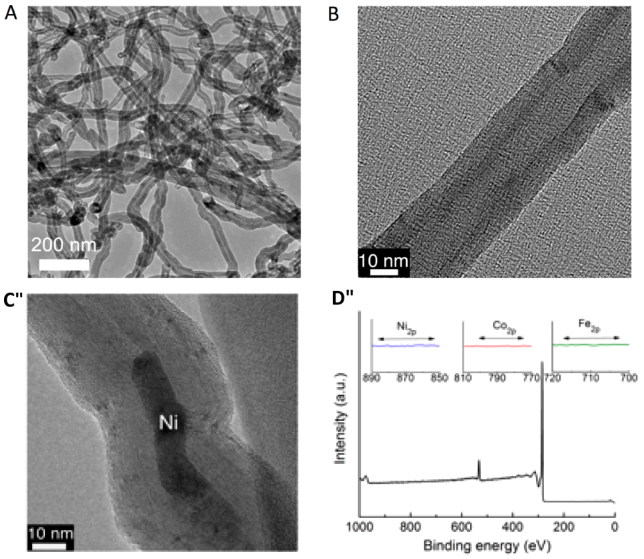

Figure 2. Elucidations of the influence of metal impurities on OER activity. (A, B) Representative TEM images of echo-MWCNTs. (C) The TEM image showing embedded metal particles in echo-MWCNTs, which have been confirmed as Ni using EDX measurements. (D) XPS survey spectra of the echo-MWCNTs. Insets are the high resolution XPS spectra of Ni_{2p}, Co_{2p} and Fe_{2p}, respectively.

echo-MWCNTs are well preserved and the residual Ni are all embedded inside MWCNTs (Figure 2C). XPS data obtained after electrochemical activation also confirm no detectable metals on the surface, except for C and O (Figure 2D). Furthermore, the characteristic oxidation peaks of Ni itself to catalytic active NiOOH species, usually observed prior to the onset of water oxidation in Ni-catalyzed OER processes,[6,30] are not detected in the polarization curves (Figure 1A). The above data suggest that the echo-MWCNTs are not etched during the electrochemical activation process, mainly attributed to the mild electrochemical activation conditions applied in the study (0−0.8 V vs Ag/AgCl, 22 °C, 1 atm).

To fully elucidate the role of Ni impurities, we further employed MWCNTs prepared from Fe catalysts with undetectable level of Ni, as revealed by ICP-MS (<1 ppb). A high OER catalytic activity was also obtained with these MWCNTs after the three-step treatments, compared with the untreated ones (Figure 3A). Previous studies have suggested that Fe is a poor OER catalyst.[6,7] STEM-EDX and XPS also confirm that no residual Fe can be detected on the surface of MWCNTs. Finally, we deliberately added Fe into the MWCNTs catalysts and prepared Fe-modified MWCNTs according to a previously described method.[11] Figure 3B, C show the SEM image and EDX elemental mapping of the obtained Fe-modified MWCNTs, where the surface of the MWCNTs has been densely decorated with Fe nanoparticles. The chemical compositions of the Fe attached on MWCNTs are Fe_2O_3 as revealed by XPS spectra (Figure S9). However, the Fe-modified MWCNTs exhibit negligible OER activity, similar to the raw MWCNTs (Figure 3A). Collectively, it can be concluded that residual metals, either Ni or Fe, make very minor contributions to the OER activity. The observed high OER catalytic activity mainly arises from nonmetallic sites on the surface of MWCNTs.

One crucial question for surface-oxidized MWCNTs being the OER catalysts, rather than the supports for metal-based catalysts, is whether they can survive in the strongly oxidative environment of OER, or themselves also will be oxidized. We investigated the

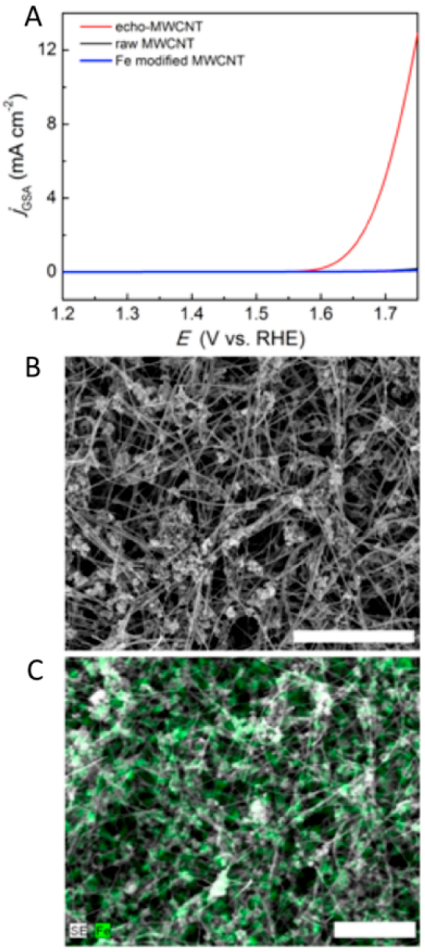

Figure 3. Elucidations of the influence of Fe impurities on OER activity. (A) RDE polarization curves obtained with echo-MWCNTs, raw MWCNTs and Fe-modified MWCNTs, using MWCNTs prepared from Fe catalysts, in 1 M KOH without *iR* compensation. (B) SEM image of the Fe modified MWCNTs. (C) The EDX image of Fe-modified MWCNTs obtained with SEM. The scale bars in B and C are 5 μm.

stability of echo-MWCNTs in OER. It is first observed that the polarization curves obtained with echo-MWCNTs before and after 100 potential cycles are identical (Figure S10A). Furthermore, we carried out constant current bulk electrolysis of water at j = 5 mA cm^{-2} using echo-MWCNTs loaded carbon fiber paper (CFP) as the working electrode. The chronopotentiometric curves (Figure 1E) shows that the potentials remain stable during the course of water electrolysis in both 0.1 and 1 M KOH. The results of bulk electrolysis of water at constant potential of 1.72 V (~10 mA cm^{-2}) using echo-MWCNTs loaded nickel foam substrate also suggests the robustness of the echo-MWCNTs catalysts without decay of electrolysis current (Figure S11). Furthermore, XPS and HRTEM characterizations of the echo-MWCNTs catalysts after >10 h bulk water electrolysis reveal that the echo-MWCNTs remain almost unchanged in chemical compositions and morphology, where no shortening, surface roughening, or unzipping of CNTs is observed (Figure S10B−D). Finally, gas chromatography is applied to detect the gas products of water electrolysis using the echo-MWCNTs catalyst. Within the detection limit of gas chromatographer (10 ppm), no CO or CO_2 (the possible oxidation products of CNTs) can be detected during the course

DOI: 10.1021/ja509879r
J. Am. Chem. Soc. 2015, 137, 2901−2907

of 5 h electrolysis of water at 5 mA cm^{-2}. These results are echoed with the high Faraday efficiency (99%) obtained by RRDE (Figure S5). The collective data confirm that the as-prepared echo-MWCNTs are durable catalysts for OER.

The three-step treatment of the MWCNTs is found to be important to obtain ample catalytic sites to mediate the reaction while preserving the structure integrity and good electrical conductivity.[10,31,32] We further investigated the factors for the catalytic performance, including (i) strength of oxidizing acids, (ii) hydrothermal process, and (iii) electrochemical activation process. First, we have explored the effect of acid strength by using stronger or weaker oxidizing acids compared to the piranha solution. To introduce more oxygen-containing groups and active sites, we apply a strong oxidization method by refluxing MWCNTs in mixtures of concentrated HNO_3 and concentrated H_2SO_4.[33] Compared with piranha solution-treated-MWCNTs, the strongly oxidized MWCNTs have more oxygen content (20 at. %, Figure S12). However, the structure integrity of MWCNTs is severely damaged showing shortened tube length and etched surface (Figure S13). Consequently, after hydrothermal annealing and electrochemical activation, the strongly oxidized MWCNTs exhibit negligible OER catalytic activity (Figure S14). Refluxing MWCNTs in concentrated HCl produces weakly oxidized MWCNTs (~1.0 at. % oxygen) (Figure S15). The OER activity of weakly oxidized MWCNTs after hydrothermal and electrochemical treatment is also significantly lower than the echo-MWCNTs prepared from piranha solution-treated, mildly oxidized MWCNTs (~4.0 at. % oxygen) (Figure S14). It has been demonstrated that piranha solution treatment enables controlled oxidation of MWCNTs by introducing relatively large amount of oxygen groups onto MWCNTs while their structure and morphologies largely maintained.[8]

Second, the hydrothermal treatment of MWCNTs is also found to be crucial for improving catalytic activity. Although the total oxygen content on ho-MWCNT (2.2 at. %) is lower than o-MWCNTs (4.0 at. %), as results of desorption of less stable oxygen groups such as (−OH) in the hydrothermal treatment at 180 °C,[34] the OER catalytic activity of ho-MWCNT is higher than o-MWCNTs. This is attributed to two possible factors: (i) increased conductivity of oxidized MWCNTs, presumably via phase transformation into prominent oxidized and graphitic domains by temperature-driven oxygen diffusion;[35] (ii) the removal of less-stable oxygen-containing groups makes more active carbon available for water oxidation since the process is mediated by substrate carbon atoms near the oxygen-containing functional groups. Third, electrochemical activation leads to significant improvement in OER activity. This is attributed to in situ oxidation of fresh defect sites in the oxidized domains on the graphitic surface after hydrothermal annealing, leading to further increase in catalytic sites and OER activity. It is worth mentioning that direct electrochemical activation of MWCNTs, without the preoxidation and/or hydrothermal steps, show very weak OER activity (Figure S16). Therefore, it is evidenced that all the three treatment methods are cooperative and indispensible for the high OER activity of echo-MWCNTs.

To identify the catalytic active sites of surface-oxidized MWCNTs for OER, we monitor the change of chemical compositions of the working surface of MWCNTs with XPS, and correlate the change with the OER activity. The change of chemical compositions can be achieved by removing the oxygen-containing groups deliberatively from ho-MWCNTs by heating ho-MWCNTs to 1000 °C at a ramping rate of 5 °C/min in an argon environment (see details in Experimental Section). A significant reduction of oxygen content from 2.2 to <1 at. % (Figure S17) is accompanied by significantly diminished OER activity (Figure 4A), suggesting oxygen-containing groups

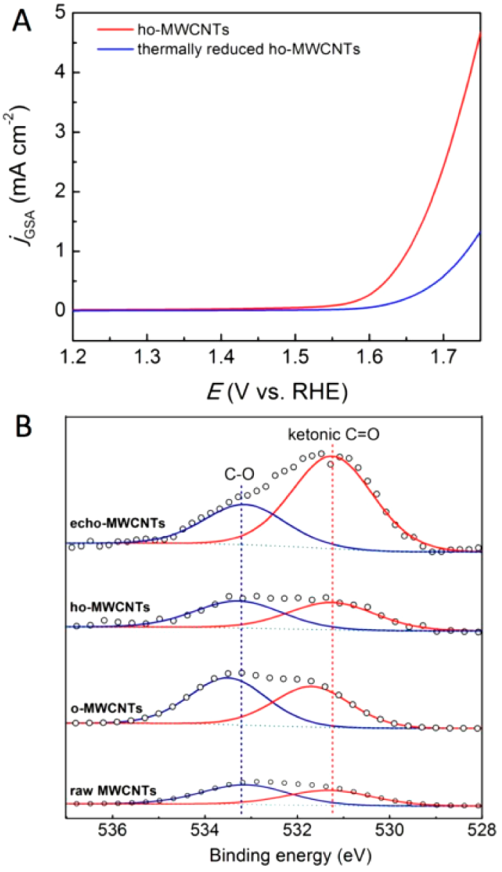

Figure 4. Identification of the catalytic active sites in echo-MWCNTs. (A) Polarization curves obtained with ho-MWCNTs (oxygen content 2.2 at. %) and thermally reduced ho-MWCNTs (oxygen content <1 at. %) in 0.1 M KOH solution at a scan rate of 5 mV s^{-1}. (B) High resolution XPS O_{1s} spectra obtained with raw MWCNTs, o-MWCNTs, ho-MWCNTs and echo-MWCNTs, respectively.

contribute significantly to the active sites. Furthermore, for every step of treatment, the change in OER catalytic activity can be correlated to the amount of ketonic C═O groups on the MWCNTs. Figure 4B shows the high resolution XPS O 1s spectra of raw MWCNTs, o-MWCNTs, ho-MWCNT and echo-MWCNTs, respectively. The oxygen functionalities on the four samples were mainly comprised of ketonic C═O (531.2 ± 0.3 eV) groups and C−O (533.1 ± 0.3 eV) (epoxide and hydroxyl) groups.[36] Relative amounts of C−O and C═O are presented in Figure 4B by the ratio of their intensities, $I_{(C-O)}/I_{(C=O)}$. Upon oxidization of raw MWCNTs in piranha solutions, the intensities of both $I_{(C-O)}$ and $I_{(C=O)}$ increase while the $I_{(C-O)}/I_{(C=O)}$ values decrease from 1.3 to 1.15. Hydrothermal treatments decrease the intensities of both bands slightly, yet more of the C−O band, decreasing the $I_{(C-O)}/I_{(C=O)}$ value further to 1.0. However, owing to enhanced conductivity and the removal of less-stable oxygen groups which makes more active carbon available for water oxidation, further enhancement in OER activity is observed. Most dramatic change in composition is observed during electrochemical treatment step with significantly increased $I_{(C=O)}$ while $I_{(C-O)}$ increased only slightly with $I_{(C-O)}/I_{(C=O)}$ = 0.4. The increase in ketonic C═O groups

DOI: 10.1021/ja509879r
J. Am. Chem. Soc. 2015, 137, 2901−2907

during electrochemical treatment is accompanied by dramatic enhancement in OER activities. The results suggest that the ketonic C═O sites make substantial contributions to the OER activity of echo-MWCNTs, while C−O bonds play a relatively minor role.

The mechanism of electrocatalytic oxidation of water over the ketonic C═O groups at echo-MWCNTs was explained by identifying possible intermediates using first-principles electrochemical calculations.[37] The Faraday efficiency obtained in RRDE measurements is close to unity (99%), which suggests that OER at the echo-MWCNTs follows a 4e oxidation mechanism. The previous theoretical studies have proposed a 4-electron oxidation reaction in alkaline media,[38,39] as represented blow:

$$H_2O(1) \rightarrow OH(ad) + H^+(aq) + e^- \quad (1)$$

$$OH(ad) \rightarrow O(ad) + H^+(aq) + e^- \quad (2)$$

$$O(ad) + H_2O(1) \rightarrow OOH(ad) + H^+(aq) + e^- \quad (3)$$

$$OOH(ad) \rightarrow O_2(g) + H^+(aq) + e^- \quad (4)$$

The effects of bias voltage (U) and pH were included in the energy diagram at different stages of oxidation. Density functional theory (DFT) calculation on periodic multi- walled nanotube is forbidden at this moment because of the huge computational demand for simulating nanotubes with 20 nm in diameter. As a remedy, we have modeled the electrochemical reactions on a $C_{130}H_{28}$ curved graphene cluster which was taken out from a (150, 150) armchair carbon nanotube of 20 nm in diameter, which is close to the outer wall of the MWCNTs used in this study. To corroborate with our functional group characterization by experiments, we studied the reactions on two kinds of oxidized curved graphene clusters. The first one contains one lactone and one ketone groups (namely GR-LK) which was proposed previously upon ozone oxidation,[40] and the second one contains two ketone groups (namely GR-KK) (Figure S18−S20).

Despite the fact that the carbon nanotube provides large specific surface area, the water oxidation reactions can only happen at the adsorption sites near the oxidized functional groups. We have considered 11 carbon atop adsorption sites for −OH, 10 C−C bridge adsorption sites for −O−, and 11 carbon atop adsorption sites for −OOH. Totally there are 34 possible reaction channels on GR-LK and 38 possible reaction channels on GR-KK. Under the same conditions as in the experiments, we have corrected the energy diagram by using the relation: $E(U, \mathrm{pH}) = E - 0.0592\ \mathrm{pH} - neU$,[37] where n is the number of electron in the half reaction. In total 34 and 38 energy diagrams for all possible reaction channels have been created. Among these possible reaction channels, only some of them can be observed which show downhill energy drop for $H_2O \rightarrow OH \rightarrow O \rightarrow OOH \rightarrow O_2$.[38,39] According to this criterion, only one reaction channel for GR-LK and two reaction channels for GR-KK were identified. Shown in Figure 5, the energy curves of these reaction channels go downhill in the course of the reaction. The previous water oxidation investigation on metal oxide surface suggested that the energy state of the −O− intermediate governed the magnitude of the thermochemical overpotential.[39] In our work, the experimentally observed low overpotential can be understood by the involvement of epoxide intermediate instead of ether intermediate, otherwise a large overpotential would be expected if −O− was trapped in the ether form.[41] Another interesting observation is that the −OH and -OOH do not adsorb at the same carbon atop adsorption site. Since a spontaneous reaction happens when the $E(U, \mathrm{pH})$ diagram goes downhill from the thermodynamical point of view, the stability of OH, O and OOH should be in the ascending order. This requires that the OH species adsorb on a less favorable adsorption site while the OOH species adsorbs on a more favorable adsorption site. For instance, on the GR-KK sample, the presence of the electron-withdrawing ketone group reduces the electron population of the carbon atoms at the meta-position, whereas the carbon atoms at the *ortho*- and *para*-positions are less affected. As shown in Figure 5B and 5C, the OH species first adsorbs at the *meta* position, and the branching reaction leads to either an *ortho*-OOH or *para*-OOH intermediate (also see Scheme S1). Indeed, our DFT calculations reveal that the OOH species cannot adsorb on the meta-carbon. Similarly, we can also observe an initial OH adsorption at the α-carbon and a later OOH adsorption at the α-carbon near the preadsorbed lactone group. Thus, our DFT calculations show that the electro-water oxidation on the echo-MWCNTs with ketonic functional groups is thermodynamically more feasible. This can be traced back to the various strengths of stabilization on the oxidation intermediates from the substrate carbon atoms with different relative positions to the ketone group.

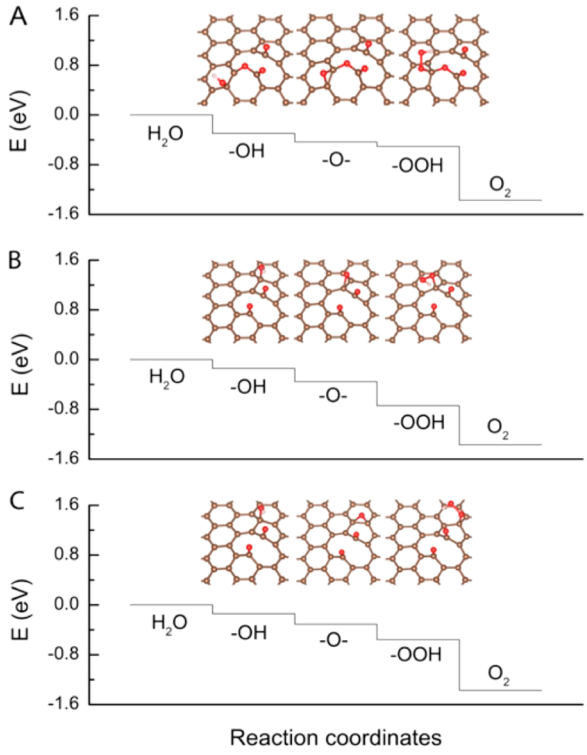

Figure 5. Energy profiles of the 4-electron water oxidation mechanism. The energy corrections due to the working voltage potential of 1.53 V and the pH value of 13 were taken into account. Water oxidation on the preoxidized graphene cluster models with (A) both lactone and ketone groups; (B) and (C) ketone groups only.

CONCLUSION

The surface oxidation of carbon nanomaterials is a decisively important process for supporting metal and metal oxide catalysts for utilizations in energy storage and conversion devices such as solar water splitting cells, and fuel cells. Toward the development of metal free electrocatalysts, the surface oxidation is also often required to produce defect sites for deliberate doping of heteroatoms into the graphitic networks. Our study discovered

DOI: 10.1021/ja509879r
J. Am. Chem. Soc. 2015, 137, 2901−2907

that surface-oxidized MWCNTs, post-treated by hydrothermal and electrochemical activation treatments, showed unprecedented OER activity even in the absence of surface metal oxide catalysts. Such an OER activity was rationalized by the oxygen-containing functional groups such as ketonic C═O, which altered the electronic distribution of the surrounding carbon atoms at the MWCNT surfaces and facilitated the adsorption of water oxidation intermediates. Our findings open the door to new applications of surface-oxidized MWCNTs for catalyzing a class of important anodic reactions in water splitting and fuel cells. Further improvement of the activity of the surface-oxidized carbon nanomaterials is expected when the structure and compositions can be tuned and/or hybrid carbon materials are used.

■ ASSOCIATED CONTENT

Supporting Information

Materials, RRDE measurements, ECAS calculations, DFT calculations and supporting data. This material is available free of charge via the Internet at http://pubs.acs.org.

■ AUTHOR INFORMATION

Corresponding Author

chuan.zhao@unsw.edu.au

Notes

The authors declare no competing financial interest.

■ ACKNOWLEDGMENTS

The authors thank UNSW Mark Wainwright Analytical Centre (MWAC) for the access of all characterization facilities, and Dr. Bin Gong from MWAC for his assistance in XPS characterizations. The authors are grateful to Dr. Chuan-Ming Tseng, at the Institute of Physics, Academia Sinica, Taiwan, for his assistance in STEM-EDX characterizations. W.L.Y. acknowledges A*STAR Computational Resource Centre (A*CRC) for computing facilities. The study was financed by an Australian Research Council (ARC) Discovery Grant (DP110102569).

■ REFERENCES

(1) Dinca, M.; Surendranath, Y.; Nocera, D. G. *Proc. Natl. Acad. Sci. U. S. A.* **2010**, *107*, 10337.

(2) Lewis, N. S.; Nocera, D. G. *Proc. Natl. Acad. Sci. U. S. A.* **2006**, *103*, 15729.

(3) Kanan, M. W.; Nocera, D. G. *Science* **2008**, *321*, 1072.

(4) Reier, T.; Oezaslan, M.; Strasser, P. *ACS Catal.* **2012**, *2*, 1765.

(5) Lee, Y.; Suntivich, J.; May, K. J.; Perry, E. E.; Shao-Horn, Y. *J. Phys. Chem. Lett.* **2012**, *3*, 399.

(6) Louie, M. W.; Bell, A. T. *J. Am. Chem. Soc.* **2013**, *135*, 12329.

(7) Smith, R. D. L.; Prevot, M. S.; Fagan, R. D.; Zhang, Z. P.; Sedach, P. A.; Siu, M. K. J.; Trudel, S.; Berlinguette, C. P. *Science* **2013**, *340*, 60.

(8) Lu, X.; Zhao, C. *J. Mater. Chem. A* **2013**, *1*, 12053−12059.

(9) Mette, K.; Bergmann, A.; Tessonnier, J. P.; Havecker, M.; Yao, L. D.; Ressler, T.; Schlogl, R.; Strasser, P.; Behrens, M. *ChemCatChem* **2012**, *4*, 851.

(10) Liang, Y. Y.; Li, Y. G.; Wang, H. L.; Dai, H. J. *J. Am. Chem. Soc.* **2013**, *135*, 2013.

(11) Liang, Y. Y.; Li, Y. G.; Wang, H. L.; Zhou, J. G.; Wang, J.; Regier, T.; Dai, H. J. *Nat. Mater.* **2011**, *10*, 780.

(12) Gong, M.; Li, Y. G.; Wang, H. L.; Liang, Y. Y.; Wu, J. Z.; Zhou, J. G.; Wang, J.; Regier, T.; Wei, F.; Dai, H. J. *J. Am. Chem. Soc.* **2013**, *135*, 8452.

(13) Tian, G. L.; Zhao, M. Q.; Yu, D. S.; Kong, X. Y.; Huang, J. Q.; Zhang, Q.; Wei, F. *Small* **2014**, *10*, 2251.

(14) Chen, S.; Duan, J. J.; Jaroniec, M.; Qiao, S. Z. *Adv. Mater.* **2014**, *26*, 2925.

(15) Zhao, Y.; Nakamura, R.; Kamiya, K.; Nakanishi, S.; Hashimoto, K. *Nat. Commun.* **2013**, *4*, 2390.

(16) Datsyuk, V.; Kalyva, M.; Papagelis, K.; Parthenios, J.; Tasis, D.; Siokou, A.; Kallitsis, I.; Galiotis, C. *Carbon* **2008**, *46*, 833.

(17) Suntivich, J.; May, K. J.; Gasteiger, H. A.; Goodenough, J. B.; Shao-Horn, Y. *Science* **2011**, *334*, 1383.

(18) Trotochaud, L.; Ranney, J. K.; Williams, K. N.; Boettcher, S. W. *J. Am. Chem. Soc.* **2012**, *134*, 17253.

(19) McCrory, C. C. L.; Jung, S. H.; Peters, J. C.; Jaramillo, T. F. *J. Am. Chem. Soc.* **2013**, *135*, 16977.

(20) Merrill, M. D.; Dougherty, R. C. *J. Phys. Chem. C* **2008**, *112*, 3655.

(21) Minguzzi, A.; Fan, F. R. F.; Vertova, A.; Rondinini, S.; Bard, A. J. *Chem. Sci.* **2012**, *3*, 217.

(22) Corrigan, D. A.; Bendert, R. M. *J. Electrochem. Soc.* **1989**, *136*, 723.

(23) Lin, Z. Y.; Waller, G. H.; Liu, Y.; Liu, M. L.; Wong, C. P. *Carbon* **2013**, *53*, 130.

(24) Ma, T. Y.; Dai, S.; Jaroniec, M.; Qiao, S. Z. *Angew. Chem., Int. Ed.* **2014**, *53*, 7281.

(25) Ma, T. Y.; Dai, S.; Jaroniec, M.; Qiao, S. Z. *J. Am. Chem. Soc.* **2014**, *136*, 13925.

(26) Chen, S.; Duan, J. J.; Jaroniec, M.; Qiao, S. Z. *Angew. Chem., Int. Ed.* **2013**, *52*, 13567.

(27) Stobinski, L.; Lesiak, B.; Kover, L.; Toth, J.; Biniak, S.; Trykowski, G.; Judek, J. *J. Alloys Compd.* **2010**, *501*, 77.

(28) Ambrosi, A.; Chua, C. K.; Khezri, B.; Sofer, Z.; Webster, R. D.; Pumera, M. *Proc. Natl. Acad. Sci. U. S. A.* **2012**, *109*, 12899.

(29) Ambrosi, A.; Chee, S. Y.; Khezri, B.; Webster, R. D.; Sofer, Z.; Pumera, M. *Angew. Chem., Int. Ed.* **2012**, *51*, 500.

(30) Lyons, M. E. G.; Brandon, M. P. *Int. J. Electrochem. Soc.* **2008**, *3*, 1425.

(31) Li, Y. G.; Zhou, W.; Wang, H. L.; Xie, L. M.; Liang, Y. Y.; Wei, F.; Idrobo, J. C.; Pennycook, S. J.; Dai, H. J. *Nat. Nanotechnol.* **2012**, *7*, 394.

(32) Wang, H. L.; Dai, H. J. *Chem. Soc. Rev.* **2013**, *42*, 3088.

(33) Lee, S. W.; Kim, B. S.; Chen, S.; Shao-Horn, Y.; Hammond, P. T. *J. Am. Chem. Soc.* **2009**, *131*, 671.

(34) Sun, T.; Zhang, Z. Y.; Xiao, J. W.; Chen, C.; Xiao, F.; Wang, S.; Liu, Y. Q. *Sci. Rep.* **2013**, *3*, 2527.

(35) Kumar, P. V.; Bardhan, N. M.; Tongay, S.; Wu, J. Q.; Belcher, A. M.; Grossman, J. C. *Nat. Chem.* **2014**, *6*, 151.

(36) Zhang, J.; Liu, X.; Blume, R.; Zhang, A. H.; Schlogl, R.; Su, D. S. *Science* **2008**, *322*, 73.

(37) Norskov, J. K.; Rossmeisl, J.; Logadottir, A.; Lindqvist, L.; Kitchin, J. R.; Bligaard, T.; Jonsson, H. *J. Phys. Chem. B* **2004**, *108*, 17886.

(38) Dau, H.; Limberg, C.; Reier, T.; Risch, M.; Roggan, S.; Strasser, P. *ChemCatChem* **2010**, *2*, 724.

(39) Man, I. C.; Su, H. Y.; Calle-Vallejo, F.; Hansen, H. A.; Martinez, J. I.; Inoglu, N. G.; Kitchin, J.; Jaramillo, T. F.; Norskov, J. K.; Rossmeisl, J. *ChemCatChem* **2011**, *3*, 1159.

(40) Yim, W. L.; Johnson, J. K. *J. Phys. Chem. C* **2009**, *113*, 17636.

(41) Chen, Z. F.; Nagase, S.; Hirsch, A.; Haddon, R. C.; Thiel, W.; Schleyer, P. V. *Angew. Chem., Int. Ed.* **2004**, *43*, 1552.

DOI: 10.1021/ja509879r
J. Am. Chem. Soc. 2015, 137, 2901−2907